ISSN: 0067-2904

Improving Properties of Tungsten Oxide Films by Gamma Ray Irradiation

Mustafa K. Hanoon, Eman M. Nasir*
Department of Physics, College of Science, University of Baghdad, Baghdad, Iraq

Received: 7/6/2022 Accepted: 8/3/2023 Published: 29/2/2024

Abstract

The deposition process and investigation of the physical properties of tungsten trioxide (WO_3) thin films before and after gamma irradiation are presented in this paper. The WO_3 thin films were deposited, using the pulse laser deposition technique, on glass substrates at laser energies of 600mJ and 800mJ. After deposition, the samples were gamma irradiated with Co^{60}. The structural and optical properties of polycrystalline WO_3 thin films are presented and discussed before and after 5kGy gamma irradiation at the two laser energies. X-ray diffraction spectra revealed that all the films consisted of WO_3 crystallized in the triclinic form; the dislocation density and lattice strain increased with the absorbed dosage of gamma irradiation. The optical constants, the average diameter and the surface roughness of the WO_3 films were calculated before and after gamma irradiation and for the two laser energies. It was found that the WO_3 thin films conductivity increased by γ-irradiated and with the increase of the laser energy.

Keywords: WO_3, structure properties, optical properties, Co^{60}. AFM

تحسين خصائص أغشية أوكسيد التنجستن بأستخدام أشعة كاما

مصطفى كريم حنون , ايمان مزهر ناصر*
قسم الفيزياء, كلية العلوم, جامعة بغداد, بغداد, العراق

الخلاصة

هذا البحث يهتم بعملية الترسيب وتقصي الخصائص الفيزيائية للأغشية الرقيقة لثلاثي أوكسيد التنكستن (WO_3) قبل وبعد التشعيع بمصدر كاما .في هذا البحث تم ترسيب اغشية WO_3 الرقيقة باستخدام تقنية الترسيب بالليزر النبضي على قواعد زجاجيةعند طاقة الليزر (600,800)mJ. بعد الترسيب, تم تشعيع العينات بالنظير المشع Co^{60}. عرضت ونوقشت الخصائص التركيبية والبصرية لأغشية WO_3 الرقيقة متعددة البلورات قبل وبعد التشعيع ب 5 كيلو جراي وعند طاقتي الليزر .أوضحت أطياف حيود الأشعة السينية أن جميع الأغشية تتكون WO_3 بلورات في شكل ثلاثي الميل ، وتزداد كثافة الخلع والانفعال الشبكي عند امتصاص جرعة أشعة جاما .نم حساب الثوابت البصرية, معدل الحجم الحبيبي و خشونة سطح اغشية قبل وبعد التشعيع ولطاقتي الليزر . وقد تبين ان كذلك, تزداد توصيلية أغشيةWO_3 الرقيقة بعد التشعيع وبزيادة طاقة الليزر .

*Email: eman.nasir@sc.uobaghdad.edu.iq

1. Introduction

Tungsten trioxide (WO_3) is a transition metal oxide semiconductor of wide band gap tunable in the range of E_g=2.5-2.8eV at room temperature. This material has been used to detect oxidizing and reducing gases [1-3]. It is applicable as catalyst, in windows for solar cells, electronic information displays and color memory devices. WO_3 is an n-type semiconductor which has been the most extensively studied material due to its electrochromic properties in the visible and IR region, high-coloration efficiency and relatively low price. WO_3 exhibits multiple polymorphs such as tetragonal (α), orthorhombic (β), monoclinic (ε and γ), triclinic (δ), and so–called pseudocubic [4]. Each of these forms exhibits different electrical, optical and magnetic behaviors, which are favorable for particular applications. WO_3 nanostructures can be prepared by various techniques such as sputtering, chemical vapor deposition, and sol-gel deposition [2]. The pulsed laser deposition (PLD) technique is a highly versatile method for thin film deposition performed by ablating a target with a high-energy pulsed laser in a controlled vacuum chamber. In particular, it is unique in that the technique allows for the deposition of a wide range of thin films [3-4]. The production of nanostructured tungsten trioxide films with great transparency for wavelengths over 500 nm, excellent adhesion to the conducting glass substrate, and substantial incident-light-to-current conversion efficiencies, when used as photo anodes in a photo electro chemical cell, are described here. Because their photo response extends to 500 nm, these WO_3 photo anodes can function under solar light irradiation, delivering photocurrents of a few milliamperes per square centimeter (corresponding to a band gap energy of 2.5 eV). Furthermore, electrochromic windows with excellent long-term stability and high coloring effectiveness may be created using a slightly modified preparation technique. It is a well-known fact that the physical characteristics of a material are altered when it is penetrated by high-energy radiation, such as gamma rays.When subjected to gamma rays, ionizing radiation is hypothesized to induce structural flaws (so-called color centers, or oxygen vacancies in oxides), which modify their density. Radiation effects are determined by the dose and the film's properties, including thickness; the higher the dose, the thinner the film and the greater the degradation. The absorption of gamma rays in thin films is mainly determined by their electronic structure, which changes due to photon interactions [4-6].

This paper aimed to investigate the properties of WO_3 at two laser energy before and after irradiation with Co^{60} source.

2. Experimental

WO_3 powder of high purity (99.99 %) (supplied by Himedia Laboratories Pvt. Ltd. India) was used to prepare WO_3 thin films. The required amount of WO_3 was weighed with an electronic balance, and then the powder was sintered in a quartz ampoule at 900°C for 5 hours. After that, the materials were grinded to a homogeneous powder and pressed with a hydraulic piston (type SPECAC) into pellets form of a diameter of 1cm and 0.5cm thickness. The PLD technique was used to prepare the thin films on glass substrates at a vacuum of (0.1333 Pa), at two energies of 800mJ and 600 mJ and 200 pulses with 6Hz. The prepared films were gamma irradiated with Co^{60} source with a dose of 5kGy at room temperature for 15 days.

The thickness of the prepared films was calculated by optical interference fringes (Fizeau fringes), and it was about (250, 300) nm. The XRD characteristics were studied with an (XRD-6000) (SHIMADZU) diffractometer Cu Kα, λ of 1.5406 Å, at a scanning speed of 2^o/min from 20^o to 80^o. The morphology of WO_3 thin films was provided using Atomic Force Microscope (Model TT-2 AFM). The optical properties were obtained using a UV-3100 spectrophotometer with a wavelength range of (190–1100 nm).

3. Results and Discussions

The structural properties were performed with XRD. The XRD patterns for WO_3 films before and after gamma irradiation for the two laser energies are shown in Figure 1. Results showed that the investigated samples of tungsten trioxide at the two laser energies have a polycrystalline structure. All the diffraction peaks for the two spectra of WO_3 films at 600mJ laser energy can be indexed to the triclinic structure with cell parameters: a=7.2800Å, b=7.4800Å, c=3.8200Å, α=90.000º β=90.000º, and γ=90.000º (which agrees with Card No.96-101-0619 (WO_3)). The intensity peaks in the WO_3 XRD pattern for laser energy of 600mJ were observed around 2θ = 23.2367, 24.3961, 26.6184, 28.8406, 33.5266, 34.2029, 35.6522, 41.6908 and 50.000, which are related to (001), (200), (120), (-111), (02-1), (2-20), (-121), and (400), respectively. While those for laser energy of 800mJ were at 2θ equal to 23.2014, 24.1824, 26.7642, 28.9329, 33.3735, 34.1997, 41.9449, 47.3666 and 50.0516 which are assigned to (001), (200), (-120), (-111), (02-1), (2-20), (-221), (002), (400), and (02-2) orientations, respectively. These correspond to the triclinic phase, as shown in Table 1 and Table 2. The *d* experimental values were calculated and compared with the *d* standard values, as listed in Table 1 and Table 2. The comparison shows that the prepared films XRD parameters almost agree with standard values of the tungsten oxides. After gamma irradiating WO_3, the structure remained the same (polycrystalline structure) but showed a change in some peak intensities, as shown in Figure 1.

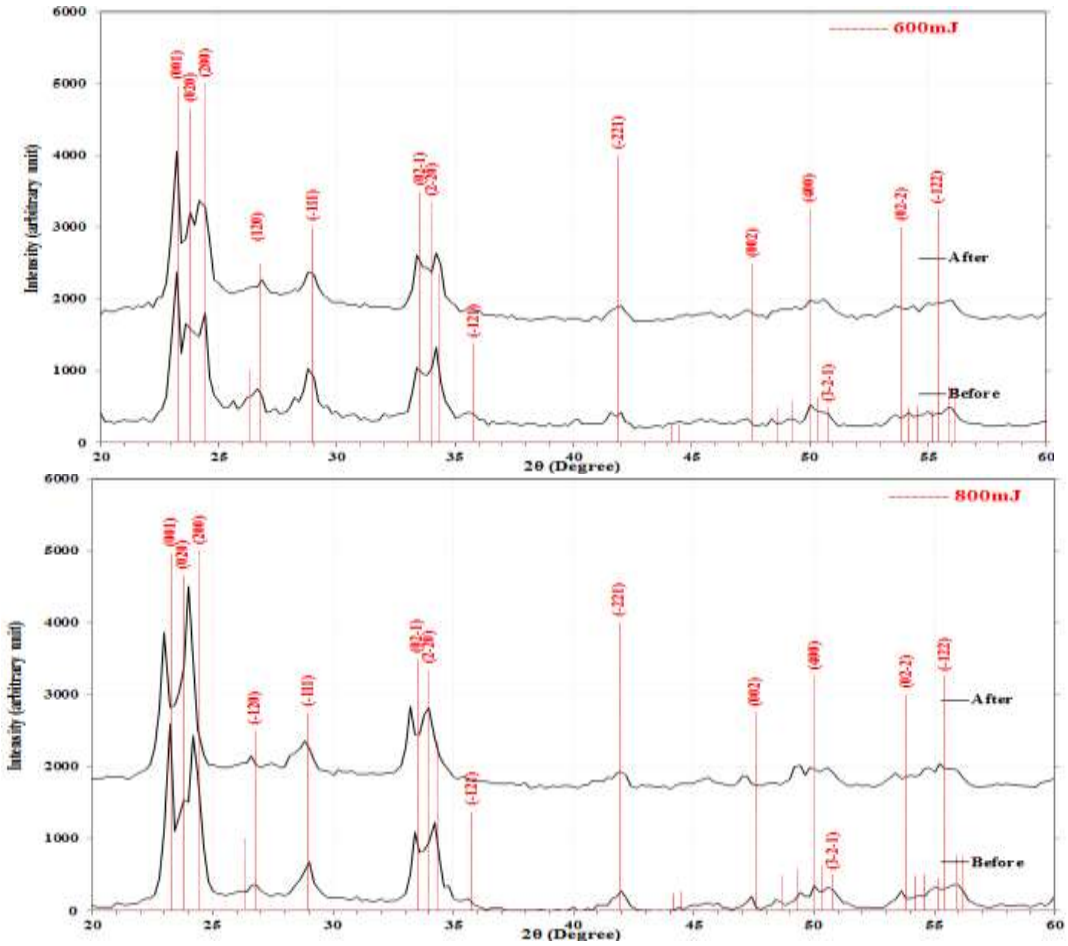

Figure 1: XRD patterns of WO_3 thin films at laser energies of (600 and 800) mJ before and after γ-irradiation

Ionization caused by gamma irradiation creates more or fewer electrons. Furthermore, it was noted that various parameters, including crystal structure alteration, temperature factors,

absorption factor, and Lorentz and polarization factor caused variations in the intensity and position of the XRD peaks. The decrease in peak intensity suggests a decrease in crystallinity [8-11]. According to several studies, the point defect caused by oxygen vacancies causes crystallinity to decrease as the overall absorbed dosage of gamma radiation increases [9-10]. After absorbing gamma radiation, the location of the conspicuous peaks migrated to the left side of the 2θ value. XRD peak shifting can be caused by lattice strain, crystal structural defects, and changes in inter-planar distance. According to Chithambararaj et al. [12], strain in the lattice structures might alter the inter-planar distance, causing the peak location to move. After gamma irradiating the WO_3 films, the inter planer distance of WO_3 for the (200) plane rises from 3.6457 Å to 3.6671 Å at 600mJ and from 3.6774Å to 3.7086Å at 800mJ. This increase in inter-planner distance denotes the occurrence of defects due to the local heat generation after radiation absorption [9, 13, and 14], as in Tables (1 and 2).

The average crystallite size was determined before and after γ-irradiation by Scherrer equation [15]:

$$D = K.\lambda/\beta\cos\theta \quad (1)$$

Where: D is the crystallite size, K is the Scherrer constant (0.9), λ is the wavelength of the X-ray used (0.15406 nm), β is the Full Width at Half Maximum ($FWHM$, radians), and θ is the peak position (radians). The average crystallite size decreased after radiation for the (001) (200) and (120) orientation at 600mJ and increased for the other peaks as in Table (1). Whereas, at 800mJ the average crystallite size dropped from (17.8) nm to (14.6) nm in (02-1) orientation and increased in some other peaks from (11.3) nm to (17.6) nm for (-120) orientation as shown in Table (2).

Table 1: X-ray diffraction parameters of WO_3 thin films at laser energy of (600) mJ before and after γ-irradiation.

Sample	2θ (Deg.)	FWHM (Deg.)	d_{hkl} (Å)	G.S (nm)	d_{hkl} Std.(Å)	□□□□nm^2) *10^{-3}	ε*10^{-3}	hkl
600mJ Before	23.2367	0.4331	3.8249	18.7	3.82	2.8516	9.191	(001))
	24.3961	0.4348	3.6457	18.7	3.64	2.8618	8.776	(200)
	26.6184	0.6280	3.3461	13.0	3.3267	5.9178	11.583	(120)
	28.8406	0.5314	3.0932	15.4	3.0821	4.1969	9.017	(-111)
	33.5266	0.5797	2.6708	14.3	2.6724	4.8818	8.397	(02-1)
	34.2029	0.4830	2.6195	17.2	2.6085	3.3768	6.850	(2-20)
	35.6522	0.8696	2.5163	9.6	2.1542	10.8591	11.800	(-121)
	41.6908	0.8212	2.1647	10.4	1.91	9.3323	9.410	(-221)
	50.0000	1.1111	1.8227	7.9	1.82	16.0675	10.397	(400)
600mJ After	23.2367	0.4848	3.8249	16.7	3.82	3.5730	10.288	(001))
	24.2512	0.5314	3.6671	15.3	3.64	4.2770	10.792	(200)
	26.8116	0.8213	3.3225	9.9	3.3267	10.1134	15.036	(120)
	28.8406	0.6280	3.0932	13.1	3.0821	5.8614	10.657	(-111)
	33.4300	0.4348	2.6783	19.1	2.6724	2.7477	6.318	(02-1)
	34.2029	0.4831	2.6195	17.2	2.6085	3.3782	6.851	(2-20)
	42.0290	0.8212	2.1481	10.4	2.1542	9.3112	9.327	(-221)
	47.4396	0.9662	1.9149	9.0	1.91	12.3983	9.595	(002)
	50.1932	1.1595	1.8161	7.6	1.82	17.4702	10.802	(400)

Table 2: X-ray diffraction parameters of WO_3 thin films at laser energy of (800) mJ before and after γ-irradiation.

Sample	2θ (Deg.)	FWHM (Deg.)	d_{hkl} Exp.(Å)	G.S (nm)	d_{hkl} Std.(Å)	□□□□□□ □□nm^2)*10^{-3}	ε*10^{-3}	hkl
800mJ Before	23.2014	0.4131	3.8306	19.6	3.82	2.5946	8.780	(001))
	24.1824	0.4648	3.6774	17.5	3.64	3.2729	9.467	(200)
	26.7642	0.7228	3.3282	11.3	3.3267	7.8346	13.257	(-120)
	28.9329	0.7228	3.0835	11.4	3.0821	7.7614	12.224	(-111)
	33.3735	0.4647	2.6827	17.8	2.6724	3.1395	6.764	(02-1)
	34.1997	0.6713	2.6197	12.4	2.6085	6.5231	9.521	(2-20)
	41.9449	0.7229	2.1522	11.8	2.1542	7.2195	8.229	(-221)
	47.3666	0.5163	1.9177	16.8	1.91	3.5422	5.136	(002)
	50.0516	0.6713	1.8209	13.1	1.82	5.8626	6.274	(400)
	53.6145	0.5163	1.7080	17.2	1.701	3.3646	4.458	(02-2)
800mJ After	22.9948	0.4131	3.8646	19.6	3.82	2.5965	8.862	(001))
	23.9759	0.4647	3.7086	17.5	3.64	3.2740	9.549	(200)
	26.6093	0.4647	3.3473	17.6	3.3267	3.2404	8.574	(-120)
	28.7780	0.9294	3.0997	8.8	3.0821	12.8414	15.807	(-111)
	33.2186	0.5680	2.6948	14.6	2.6724	4.6943	8.309	(02-1)
	33.9931	0.5164	2.6352	16.1	2.6085	3.8643	7.372	(2-20)
	41.8417	0.8778	2.1572	9.7	2.1542	10.6523	10.019	(-221)
	47.1601	0.5679	1.9256	15.3	1.91	4.2924	5.677	(002)
	49.9484	0.9294	1.8244	9.4	1.82	11.2468	8.707	(400)
	53.4079	0.8778	1.7141	10.1	1.701	9.7435	9.7435	(02-2)

When a high-energy gamma photon interacts with the WO_3 crystal, it causes atomic displacement and/or ionization, which are thought to cause crystallite size reductions for some peaks [16]. When a gamma photon interacts with a triclinic polycrystalline structure of tungsten trioxide nanomaterial, it transfers kinetic energy into the crystals 'lattice sites, causing lattice vibration and micro-stress. This causes local heating by causing lattice phonon scattering [9, 16]. The increase in crystallite size for some peaks is due to defects created by the exposure to gamma radiation. The values of dislocation density and strain increases after gamma radiation for the plain (-120) are shown in Tables 1 and 2.

Figure 2 shows the transmittance (T), and absorbance (A) spectra for un-irradiated and gamma-irradiated WO_3 films at laser energies of 600mJ and 800mJ. Figure 2(a,b) represents the absorbance spectral behavior (A) for un-irradiated and gamma-irradiated WO_3 films at laser energies of 600mJ and 800mJ. It is observed that absorbance increases with the increase of the laser energy, and after γ-irradiation as in Table 3, The near-infrared absorbance bands are greater than the UV absorbance bands, indicating that the produced WO_3 films are acceptable for solar cell and photo applications. With γ- irradiation and the increase of the laser energy, the fundamental absorption edge shifted slightly to higher wavelengths and the intensity of the transmittance spectra was reduced (as noted in Figure 2(c,d) and Table 3). This is due to transitions at localized states in the energy gap. It was also observed that the gamma-irradiation slightly shifted the transmission edge towards higher wavelengths indicating a decrease in the optical energy gap value. The optical band gap energy decrement by γ- irradiation indicates the

formation of `defects, i.e. vacancies or disorders in WO_3 films. Some atoms in the nanostructure can be lost during gamma interaction with matter; As a result, a point defect has been created. Localized states in the band gap resulted from this crystal defect, moving Fermi's level to the conduction band, which acts as a recombination center [17]. As a result, conductivity rises by decreasing the optical band gap energy of the produced films.

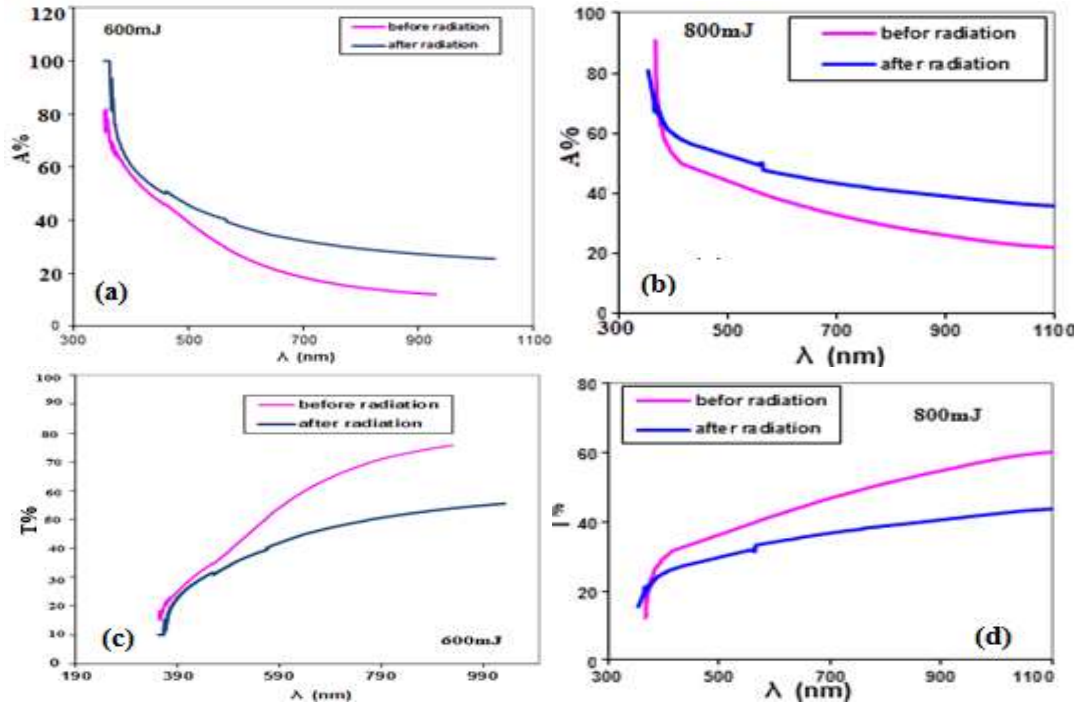

Figure 2: Transmittance (T) and absorbance (A) vs. wavelength for un-irradiated and gamma irradiated WO_3 thin films at laser energies of (600 and 800) mJ.

The absorption coefficient (α) was calculated by the following equation:

$$\alpha=2.303A/t \quad (2)$$

The absorption coefficient showed an exponential dependence on photon energy, as shown in Figure 3(a,b). It increased from 3.006 $x10^4cm^{-1}$ before irradiation to 3.502 $x10^4cm^{-1}$ after irradiation for laser energy 600mJ and increased from 3.82 $x10^4cm^{-1}$ before irradiation to 4.35 $x10^4cm^{-1}$after irradiation for laser energy 800mJ at 500 nm. The extinction coefficient (k), which varies from 0.127 to 0.148, indicates how light is absorbed as it passes through the material. Figure 3(c,d) showes a reduction in extinction coefficient as the wavelength of the films increased [19]. Both the absorption and the extinction coefficients have increased after gamma irradiation.

.

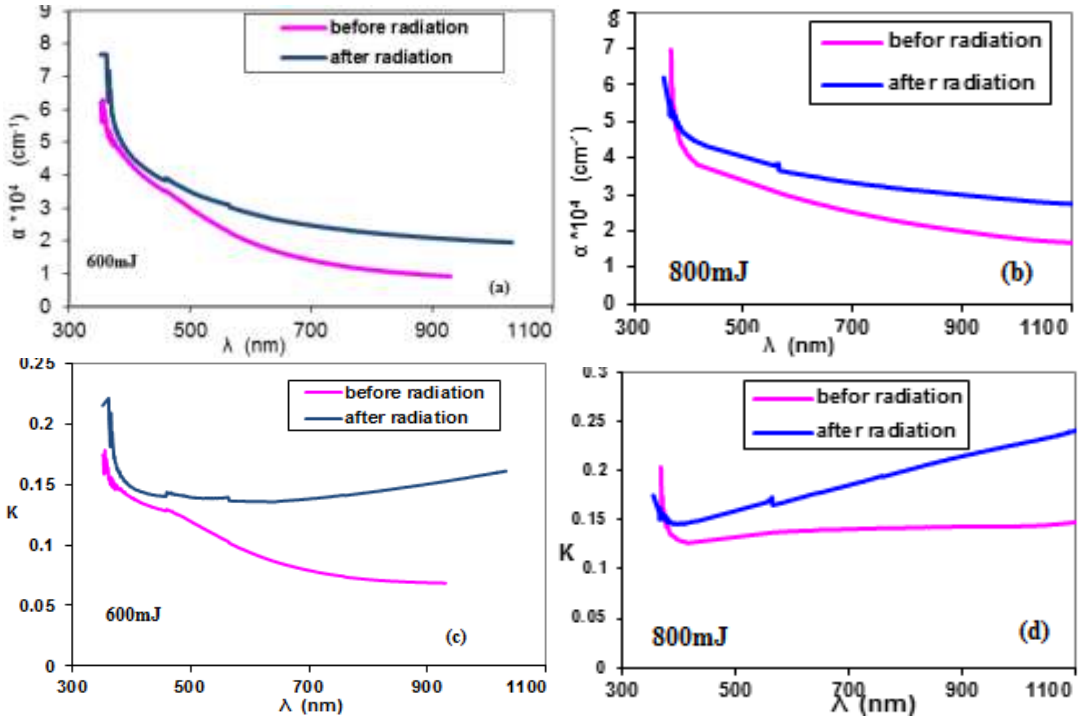

Figure 3: (a,b) absorption coefficient, **(c, d)** extinction coefficients with wavelength of un-irradiated and gamma irradiated WO_3 thin films at laser energies of (600 and 800)mJ

The optical band gap energy was calculated using Tauc equation [3,16]:

$$(\alpha h\nu) = cons.(h\nu - Eg)^r \quad (3)$$

Figure 4(a,b) displays a graph of $(\alpha h\upsilon)^2$ vs the photon energy ($h\upsilon$) at laser energies of (600 and 800)mJ of un-irradiated and gamma irradiated WO_3 thin films. The plots show straight-line regions where $\alpha \geq 10^{-4}$ cm^{-1} indicating a direct transition. Table 3 shows the band gap energy(Eg) values calculated by projecting the straight part of the plot onto the energy axis at $(\alpha h\upsilon)^2 = 0$. The value was 3.2 eV for un-irradiated WO_3 films and 3 eV after irradiation at a laser energy of 600 mJ, and 2.71 eV for un-irradiated WO_3 films, 2.38 eV after irradiation at a laser energy of 800 mJ. It is observed that the band gap energy values decreased with the increases in laser energy and with gamma irradiation. This decrease in the optical band gap energy is probably due to the increase in the energy width of the band tails of localized states, as in Figure 4(c,d) and Table 3. Similar observations have also been reported by other workers[15]. Also, the reduction in the band gap energy of WO_3 films caused by irradiation might be due to the formation of defects induced by vacancies of oxygen, which leads to the formation of localized states in the nanoparticles. In addition, gamma irradiation caused largely vacancies of oxygen and, in certain cases, stoichiometry deformation in the crystal structure [16].

As a result, a plot of ln(α) vs. hυ should be linear, and the slope is used to calculate the Urbach energy (Eu). The change of ln(α) vs. hυ of WO_3 thin films is seen in Figure 4(c,d). The reverse gradient of the linear section of these curves was used to determine Urbach energy. Table 3 shows the results of the calculations. It increased from 0.203 eV before irradiation to 0.269 eV after irradiation at a laser energy of 800mJ; the un-irradiated film has lower Urbach energy than the irradiated film, and the Urbach energy increased with the increase of the laser energy, indicating the creation of defect states in the band gap and an increase in disorder. The

Urbach band tail is caused by carrier-phonon interaction and structural disturbance. The Urbach energy values change inversely with the optical band gap energy [17].

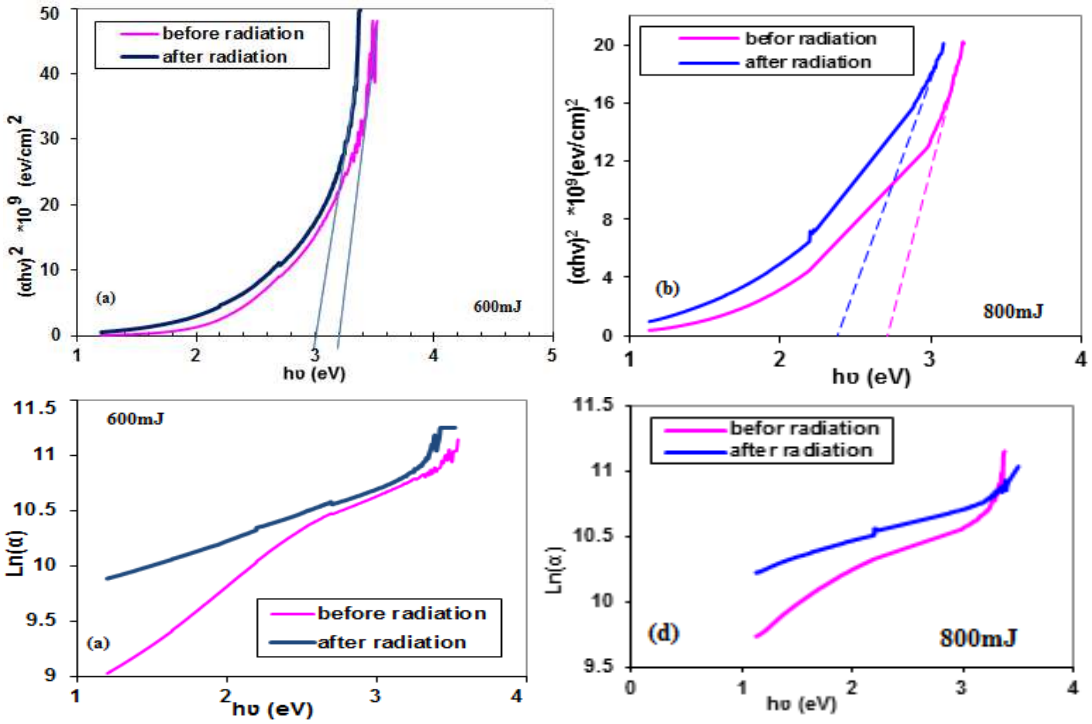

Figure 4: (a,b) optical energy gap by Tauc plot of $(\alpha h\upsilon)^2$ vs. photon energy ($h\upsilon$) **(c,d)** The optical Urbach energy of Ln (α) vs. photon energy ($h\upsilon$) of un-irradiated and gamma irradiated WO_3 thin films at laser energies of (600 and 800)mJ

Figure 5 represents the refraction index (n) and the optical conductivity ($\sigma_{optical}$) of un-irradiated and gamma irradiated WO_3 thin films at two laser energies of (600 and 800) mJ. They were calculated using the following equations:

$$R=1-(A+T) \quad (4)$$

$$n=(4R/(R-1)^2 - k^2)^{1/2} - (R+1)/(R-1) \quad (5)$$

$$\sigma_{optical}=\alpha nc/4\pi \quad (6)$$

The variation of n as a function of wavelength for un-irradiated and gamma irradiated films is shown in Figure 5(a,b). It was found that (n) decreased with wavelength and laser energy and gamma irradiation. At λ=500nm n decreased from 2.535 for un-irradiated film to 2.458 for irradiated film for laser energy of 600mJ, and from 2.36 for un-irradiated film to 2.17 for irradiated film for laser energy of 800mJ, as shown in Table 3. The slight change in refractive index is related to the modification of optical density by the gamma irradiation and laser energy.

The optical conductivity is shown in Figure 5(c,d). The results illustrate that the optical conductivity of films have significantly changed due to their exposure to gamma irradiation and to variation of laser energy, as seen in Table 3. It varied with gamma radiation from (2.05-2.15) $x10^{14}(S^{-1})$ and (2.159-2.257) $x10^{14}(S^{-1})$ for laser energies of 600mJ and 800mJ, respectively. Figure 6(a, b) shows the variation of real part of dielectric constant (ε_r) and Figure 6(c, d) shows the imaginary part of dielectric constant (ε_i) as a function of the wavelength for laser energies of 600mJ and 800mJ [13]. They were calculated using the equations:

$$K=\alpha\lambda/4\pi \quad (7)$$

$$\varepsilon_r= n^2-k^2 \quad (8)$$

$$\varepsilon_i = 2nk \quad (9)$$

As shown in Table 3, the (ε_r) values of irradiated films are lower than those of un-irradiated films, and the (ε_i) values of un-irradiated films are lower than those of irradiated films. This might be attributed to differences in internal strain, crystallite size, and stoichiometry of films [13-19].

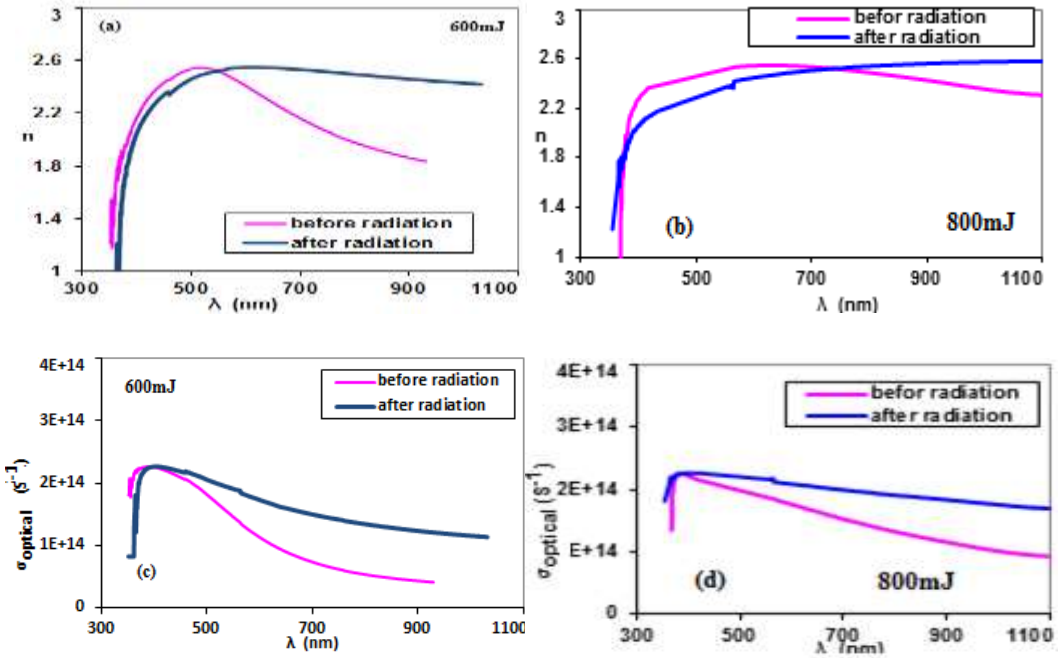

Figure 5 : (a,b)Refractive index vs. wavelength (c,d) optical conductivity vs. wavelength for un- irradiated and gamma irradiated WO_3 thin films at laser energies of (600 and 800)mJ.

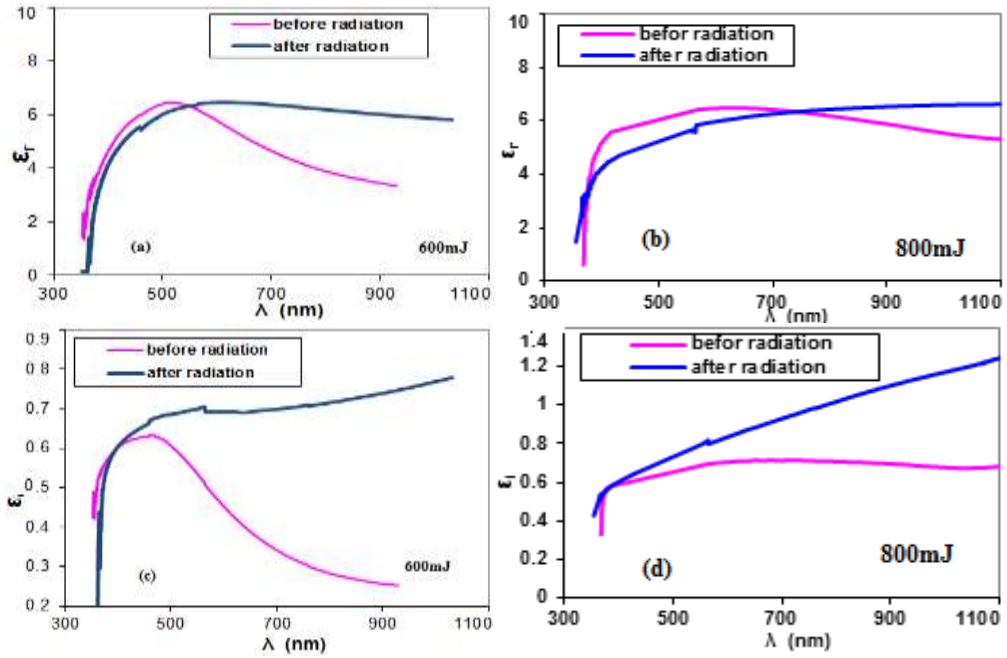

Figure 6 : The variation of (a,b) ε_r and (c,d) ε_i as a function of the wavelength for un-irradiated and irradiated WO_3 thin films at laser energies of (600 and 800)mJ.

Table 3: Values of optical band gap, Urbach energy, and optical constants of un-irradiated and irradiated WO_3 thin films, at λ=500nm for laser energies of (600 and 800)mJ.

Laser Energy	γ-irradiation	A	T	α×10^4 (cm)$^{-1}$	E_g (eV)	E_u (eV)	k	n	ε_r	ε_i	σ optical (S^{-1})x10^{14}

(mJ)											
600	Before	0.391	0.406	3.006	3.2	0.161	0.119	2.535	0.606	6.413	**2.05**
	After	0.456	0.349	3.502	3	0.227	0.139	2.458	0.685	6.026	**2.15**
800	Before	0.497	0.318	3.82	2.71	0.203	0.127	2.36	0.60	5.59	**2.159**
	After	0.566	0.271	4.35	2.38	0.269	0.148	2.17	0.65	4.71	**2.257**

Figure 7 shows the surface morphology of the WO_3 films as studied by the AFM for un-irradiated and gamma irradiated films with two laser energies of (600 and 800)mJ. The AFM images show clearly that gamma irradiation affects the surface morphology of WO_3 films in a substantial way, with grain structure and well-defined grain boundaries. As seen from the micrographs in 3D, the surface of the film before irradiation is uniform and rough, netted with crystal grains and consists of nano-sized grains. The roughness and average grain size of un-irradiated and gamma irradiated WO_3 thin films are given in Table 4. From Figure 7, it is seen that the roughness and grain size of the thin films changed with irradiation and laser energy. Probably, this change in grain size and surface roughness with irradiation and laser energy is attributed to an atomic rearrangement that occurs resulting in increased atom mobility on the substrate's surface with irradiation, resulting in the production of bigger grains.

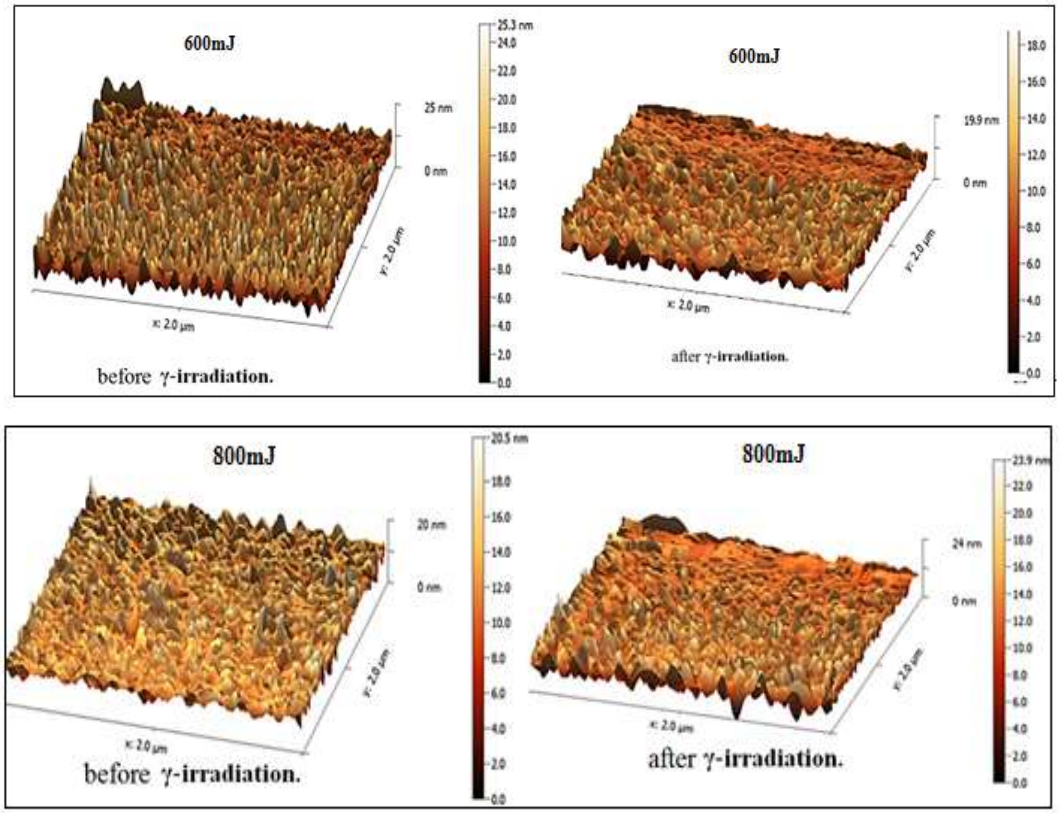

Figure 7 : AFM surface morphology in 3D of the WO_3 films for un-irradiated and gamma irradiated films at laser energies of (600 and 800)mJ

Table 4 : Roughness, average diameter and RMS of (WO_3) thin films for un-irradiation and gamma irradiation at laser energies of (600 and 800)mJ.

Laser Energy (mJ)	γ-irradiation	Roughness(nm)	Average Diameter(nm)	Root mean square(nm)
600	Before	1.41	11.83	1.87
	After	1.39	11.21	2.01
800	Before	1.34	11.66	1.74
	After	1.46	12.21	1.96

The electrical resistivity (ρ) was calculated using the following equation:

$$\rho = RA/L \quad (10)$$

The electrical conductivity (σ) increased exponentially with increasing the temperature, as illustrated in Figure 8(a,b). The Arrhenius equation is used to calculate thermally activated conductivity [18]:

$$\sigma = \sigma_o \exp(E_a/K_bT) \quad (11)$$

Where: σ_o represents the exponential factor, E_a is the activation energy, and k_b denotes Boltzman constant. The graph of ln(σ) along the y-axis against 1000/T along the x-axis, has two linear parts, as seen in Figure 8(c,d). The low and high temperature regions have independent slopes showing the signatures of two different conduction processes. The departure from the linear fit of this graph shows that the conductivity mechanism during a thermally activated system is not dominant at low temperatures [18]. This response indicates that the resulting WO_3 films have the same semiconducting properties as all WO_3 films before and after irradiation. The increase in conductivity might be attributed to the release of electrons or ions in the irradiated WO_3 as well as the internal stress [20]. The conductivity of irradiated WO_3 thin films at a laser energy of 800mJ and 600mJ was greater than that of the un-irradiated films, also the conductivity increased with increasing the laser energy from 600mJ to 800 mJ as shown in Figure 8 and Table 5. The activation energy E_{a1} and E_{a2} for WO_3 films decreased after gamma irradiation; it also decreased with the increase of the laser energy, as seen in Table 5. This may be due to the increase in absorption and the decrease in energy gap with gamma irradiation and as the laser energy increased [2-20].

Table 5: D.C. conductivity parameters of WO_3 for un-irradiated and gamma irradiated films at laser energies of (600 and 800) mJ

Laser Energy (mJ)	Gamma irradiation	$\sigma_{R.T}$ $(\Omega.cm)^{-1}$	E_{a1} (eV)	Temp. Range (K)	E_{a2} (eV)	Temp. Range (K)
600	before	$1.18x10^{-6}$	0.72	363-473	0.323	363-473
	after	$1.36x10^{-5}$	0.48	373-473	0.178	373-473
800	before	$1.74x10^{-5}$	0.236	303-363	0.354	363-473
	after	$3.72x10^{-4}$	0.129	303-373	0.051	373-473

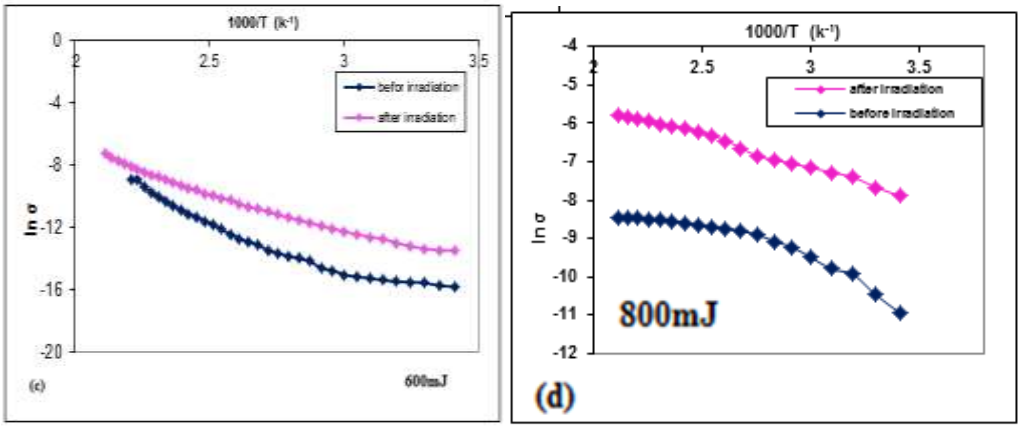

Figure 8: Arrhenius plot of the conductivity for the un-irradiated and gamma irradiated WO_3 thin films at laser energies of (600 and 800)mJ.

4. Conclusions

The impacts of Co^{60} irradiation and laser energy on the structural, morphological, optical, and electrical characteristics of WO_3 thin films created by the pulse laser deposition were investigated. The X-ray diffraction patterns of WO_3 thin films showed that all the produced films had a triclinic crystal structure. The effect of laser energy and gamma radiation dose of (5 kGy) on the crystallite size showed an irregular pattern; it decreased and increased for some peaks and was constant for others. Irradiation increased dislocation density and lattice strain, indicating that the material's disorder had grown. The AFM analysis showed that the grain size and surface roughness of the WO_3 films were affected by the irradiation of the films and the laser energy, and then increased with laser energy and gamma radiation. After gamma-irradiation and increasing the laser energy, the absorption spectra were slightly shifted to a higher wavelength. After irradiation, the Eg value of the WO_3 thin film clearly showed a slight decrease, which might be due to structural flaws. WO_3 thin films that have been γ-irradiated and at the high laser energy have a greater conductivity than films that have not been irradiated. It was concluded that it is possible to obtain better results if the value of the radiation dose and the irradiation time is increased. These findings might indicate that synthesized WO_3 will be a potential choice for optoelectronic devices.

References

[1] S. Vallejos, V. Khatko, J. Calderer, I. Gracia, C. Cané, E. Llobet, and X. Correig, "Micro-machined WO_3-based sensors selective to oxidizing gases," *Sensors and Actuators B: Chemical*, vol. 132, no. 1, pp. 209–215, 2008.

[2] Mahshad Alaei, Ali Reza Mahjoub, Alimorad Rashidi, "Preparation of Different WO_3 Nanostructures and Comparison of Their Ability for Congo Red Photo Degradation," *Iran. J. Chem. Chem. Eng*, vol. 31, no. 1, pp. 31-36, 2012.

[3] Y. S. Zou, Y. C. Zhang, D. Lou, H. P. Wang, L. Gu, Y. H. Dong, K. Dou, X. F. Song, and H. B. Zeng, "Structural and optical properties of WO_3 films deposited by pulsed laser deposition," *Journal of Alloys and Compounds*, vol. 583, pp. 465–470, 2014.

[4] Ch. Prameela and K. Srinivasarao, "Characterization of $(MoO_3)_x$ - $(WO_3)_{1-x}$ Composites," *International Journal of Applied Engineering Research*, vol. 10, no. 4, pp. 9865-9875, 2015.

[5] E. M. Nasir, "Thickness and gamma-ray effect on physical properties of CDO thin films grown by pulsed laser deposition," *Iraqi Journal of Physics (IJP)*, vol. 14, no. 29, pp. 90–100, 2019.

[6] C. Santato, M. Odziemkowski, M. Ulmann, and J. Augustynski, "Crystallographically oriented mesoporous wo3 films: synthesis, characterization, and applications," *Journal of the American Chemical Society*, vol. 123, no. 43, pp. 10639–10649, 2001.

[7] S. K. Sen, M. S. Manir, S. Dutta, M. H. Ali, M. N. I. Khan, M. A. Matin, and M. A. Hakim, "Influence of total absorbed dose of co-60 γ-radiation on the properties of H-moo3 thin films," *Thin Solid Films*, vol. 693, p. 137700, 2020.

[8] C. Nefzi, N. Beji, M. Souli, A. Mejri, S. Alleg, and N. Kamoun-Turki, "Effect of gamma-irradiation on optical, structural and electrical properties of In_2O_3: F thin films for photocatalysis application," *Optics & Laser Technology*, vol. 112, pp. 85–92, 2019.

[9] S. Kaya and E. Yilmaz, "Modifications of structural, chemical, and electrical characteristics of Er_2O_3/Si interface under Co-60 Gamma irradiation," *Nuclear Instruments and Methods in Physics Research Section B: Beam Interactions with Materials and Atoms*, vol. 418, pp. 74–79, 2018.

[10] S. Kaya, S. Abubakar, and E. Yilmaz, "Co-60 gamma irradiation influences on device characteristics of n-SnO_2/P-Si heterojunction diodes," *Nuclear Instruments and Methods in Physics Research Section B: Beam Interactions with Materials and Atoms*, vol. 445, pp. 63–68, 2019.

[11] E. M. Nasir, M. F. A. Alias, and A. N. Mohammed Ali, "The influence of x ratio and annealing temperatures on structural and optical properties for $(cuo)_x(zno)_{1-x}$ composite thin films prepared by PLD," *IOP Conference Series: Materials Science and Engineering*, vol. 757, no. 1, p. 012053, 2020.

[12] A. Chithambararaj, N. S. Sanjini, A. C. Bose, and S. Velmathi, "Flower-like hierarchical H-MoO_3: New findings of efficient visible light driven Nano photocatalyst for methylene blue degradation," *Catalysis Science & Technology*, vol. 3, no. 5, p. 1405, 2013.

[13] V. A. Doss, A. Chithambararaj, and A. C. Bose, "Effect of reaction atmosphere on structural and optical properties of hexagonal molybdenum oxide (H-MoO_3)," *AIP Conference Proceedings*, vol. 1731, no. 1, p. 050049, 2016.

[14] I. G. Madiba, N. Émond, M. Chaker, F. T. Thema, S. I. Tadadjeu, U. Muller, P. Zolliker, A. Braun, L. Kotsedi, and M. Maaza, "Effects of gamma irradiations on reactive pulsed laser deposited vanadium dioxide thin films," *Applied Surface Science*, vol. 411, pp. 271–278, 2017.

[15] H. H. Abbas and B. A. Hasan, "The effect of silver oxide on the structural and optical properties of ZnO: AgO thin films," *Iraqi Journal of Science*, vol. 63, no. 4, pp. 1526–1539, 2022.

[16] U. Gurer, O. Yilmaz, H. Karacali, S. Kaya, and E. Yilmaz, "Co-60 gamma radiation influences on the electrochemical, physical and electrical characteristics rare-earth dysprosium oxide (Dy_2O_3)," *Radiation Physics and Chemistry*, vol. 171, p. 108684, 2020.

[17] S. K. Khamari, V. K. Dixit, T. Ganguli, S. Porwal, S. D. Singh, S. Kher, R. K. Sharma, and S. M. Oak, "Effect of ^{60}Co γ-ray irradiation on electrical properties of GaAs epilayer and gaas P–I–N diode," *Nuclear Instruments and Methods in Physics Research Section B: Beam Interactions with Materials and Atoms*, vol. 269, no. 3, pp. 272–276, 2011.

[18] I. K. abd Karem and S. A. Hamdan, "The influence of CeO_2 concentration on some physical properties of Y_2O_3 thin films," *Iraqi Journal of Science*, vol. 63, no. 6, pp. 2482–2491, 2022.

[19] E. M. Nasir, H. K. Al-Lamy, H. J. Abdul-Ameer, "Optical properties of CdSe films at different thickness and annealing temperatures," *Chalcogenide Letters*, vol. 16, no. 10, pp. 485–497, 2019.

[20] E. M. Al-Fawadi, "The effect of doping ratio on the optical properties of CdSe films," *Um-Salama Science Journal*, vol. 3, no. 1, pp. 180-186, 2006.